THE JOURNAL OF PHYSICAL CHEMISTRY B

Article

pubs.acs.org/JPCB

Relative Binding Affinities of Monolignols to Horseradish Peroxidase

Amandeep K. Sangha,*[,†,‡] Loukas Petridis,[†] Xiaolin Cheng,[†,‡] and Jeremy C. Smith[†,‡]

[†]UT/ORNL Center for Molecular Biophysics, Oak Ridge National Laboratory, Oak Ridge, Tennessee 37831, United States

[‡]Department of Biochemistry and Cellular and Molecular Biology, University of Tennessee, Knoxville, Tennessee 37996, United States

Supporting Information

ABSTRACT: Monolignol binding to the peroxidase active site is the first step in lignin polymerization in plant cell walls. Using molecular dynamics, docking, and free energy perturbation calculations, we investigate the binding of monolignols to horseradish peroxidase C. Our results suggest that *p*-coumaryl alcohol has the strongest binding affinity followed by sinapyl and coniferyl alcohol. Stacking interactions between the monolignol aromatic rings and nearby phenylalanine residues play an important role in determining the calculated relative binding affinities. *p*-Coumaryl and coniferyl alcohols bind in a pose productive for reaction in which a direct H-bond is formed between the phenolic −OH group and a water molecule (W2) that may facilitate proton transfer during oxidation. In contrast, in the case of sinapyl alcohol there is no such direct interaction, the phenolic −OH group instead interacting with Pro139. Since proton and electron transfer is the rate-limiting step in monolignol oxidation by peroxidase, the binding pose (and thus the formation of near attack conformation) appears to play a more important role than the overall binding affinity in determining the oxidation rate.

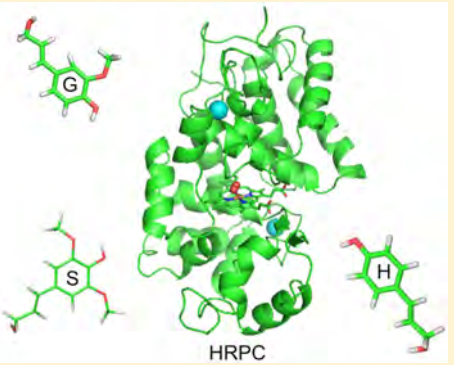

INTRODUCTION

Lignin is a complex polymer derived mainly from three phenylpropanoid monomers: *p*-coumaryl (H), coniferyl (G), and sinapyl (S) alcohols, also called monolignols[1] (Figure. 1).

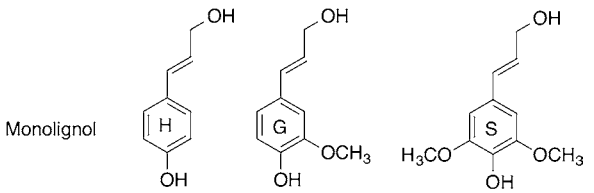

Figure 1. Three main monolignols that constitute lignin structure.

Lignin is present in the secondary cell wall of plants, providing mechanical support and regulating water conduction, and also plays a crucial role in hindering plant deconstruction to biofuels and bioproducts.[2,3] Reducing lignin content in plants or altering its structure has shown promise for improving efficiency in biofuel and bioproduct production.[4−7] Therefore, understanding lignin polymerization and structure is important both for fundamental reasons and for devising rational strategies to overcome resistance of plant biomass to industrial conversion.[8,9]

Many factors determine the structure of plant lignin, including the relative rates of monolignol synthesis,[4,6,7,10] their transport across membranes,[11,12] binding to and oxidation by peroxidase enzymes,[13,14] and radical coupling reaction enthalpies for various types of interunit bonds.[15]

Lignin polymerization, catalyzed by peroxidases and laccases, takes place in three steps: monolignol binding to the enzyme active site, H_2O_2-mediated oxidation at the active site to form radicals, and finally radical coupling reactions to form lignin polymers.[16,17] In previous studies on the radical coupling reactions it was shown that the three monolignols favor specific interunit linkage types for self- and cross-coupling reactions during lignin polymerization.[15] The oxidation rates of the monolignols and other lignin precursors are dependent on their chemical composition.[18]

Two monolignol molecules are oxidized during one oxidation cycle, the second oxidation being the rate-limiting step, 10 times slower than the first.[19] Crystal water W2 and residues His42 and Arg38 play important roles during peroxidase oxidation (Figure. 2). W2 is hydrogen-bonded to the phenolic group on the substrate monolignol. The substrate phenolic group acts as a proton donor and W2 as an acceptor in this hydrogen bond that facilitates proton transfer during the oxidation process.[20]

Knowledge about the monolignol binding is crucial for understanding lignification in plant cell walls. However, this

Received: January 24, 2016
Revised: July 21, 2016
Published: July 22, 2016

DOI: 10.1021/acs.jpcb.6b00789
J. Phys. Chem. B 2016, 120, 7635−7640

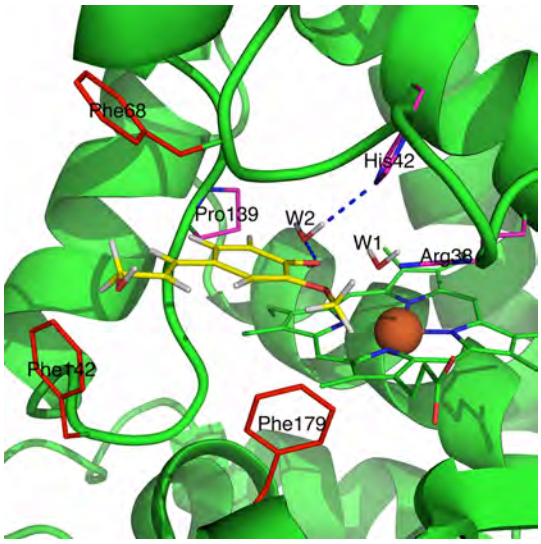

Figure 2. Crystal structure of HRPC (6ATJ.pdb). Coniferyl alcohol (yellow) bound to the active site of horseradish peroxidase C. The heme group is in its resting state and contains an iron atom (orange). Important residues His42, Arg38, and Pro139 are in magenta, and crystal waters (W1 and W2) involved in binding and oxidation of the monolignols are also shown. Three phenylalanine residues, 68, 142, and 179 (red), guard the entrance of active site. W2 forms H-bonds (dashed blue lines) with His42 and the phenolic −OH of coniferyl alcohol.

first step of monolignol binding to the enzyme active site remains unexplored to date. Here we study monolignol binding (the structure and the specificity) to the resting state of horseradish peroxidase C (HRPC) using docking calculations. Further, we quantify the relative binding affinities of the three primary monolignols to the resting state of HRPC in their productive poses for oxidation using molecular dynamics (MD) free energy perturbation (FEP)[21−24]simulations. Collectively, these results suggest that although binding affinity of the coniferyl alcohol is least favorable, its binding pose is most suitable for the oxidation reaction among the three monolignols studied here.

COMPUTATIONAL METHODS

Molecular Dynamics and Free Energy Perturbation Simulations. The initial structure for the MD-FEP simulations was obtained from a substrate-bound crystal structure (PDB access code 6ATJ) of HRPC.[13] The crystallographic ferulic acid was converted to coniferyl alcohol with the allylic hydroxyl group pointing to the allylic double bond, this being the lowest energy conformer of coniferyl alcohol.[15] There are three orientations of ferulic acid in the crystal structure (Figure SI2).[25] The first (pose A), with an occupancy of 0.46, has the phenolic hydroxyl group oriented away from the heme Fe. The second (pose B), with its allylic side chain inside the active site, is biologically inactive and has the lowest occupancy (0.26). The third orientation (pose C) with the phenolic hydroxyl pointed toward the heme Fe and an occupancy of 0.36 was chosen here, as it is the only geometry that allows oxidation.[20]

The protein was embedded in a cubic water box of 76 × 84 × 71 Å^3 dimensions. The system was neutralized using chloride ions. All systems were prepared with VMD,[26] and simulations were performed with NAMD2.9.[27] The CHARMM22 force field[28] with CMAP corrections[29] and the TIP3P water model[30] were used to describe the protein and solvent, respectively. Parameters for *p*-coumaryl, coniferyl and sinapyl alcohols (see Supporting Information) were assigned by analogy from the CHARMM lignin[31] and General force fields.[32] In the resting state of the HRPC, the heme Fe is 5-coordinated, and the distal histidine (His170) is bonded to the heme Fe such that the Fe is slightly out of the plane of the prosthetic group. Parameters for 5-coordinated heme are provided in Table SI1.

Before starting the FEP simulations, the system was first energy minimized for 15 000 steps while keeping the protein backbone, the heavy atoms of the heme and monolignol, and the calcium ions fixed. Then, the system was energy minimized for another 5000 steps without fixing atoms. Starting from 0 K, the temperature of the system was raised to 300 K in increments of 20 K using MD, simulating the system at each temperature for 20 ps while the Cα of the protein, the heavy atoms in the heme and the monolignol, and calcium ions were harmonically restrained using a force constant of 1.0 kcal/(mol Å). At 300 K, all the restraints were released, and the system was further equilibrated for 20 ps before starting the FEP simulations.

All MD-FEP simulations were carried out in the NPT ensemble. The temperature was maintained at 300 K using Langevin damping with a friction coefficient of 1 ps^{-1}, and the pressure was maintained at 1 bar using the Langevin piston method.[33] Periodic boundary conditions were applied. A time step of 2 fs was used throughout the simulations. Nonbonded interactions were calculated at every time step. PME was used to calculate long-range electrostatic interactions every two time steps.[34] Lennard-Jones and short-range Coulombic interactions were truncated smoothly at 12 Å with a switching function applied at 10 Å. The SHAKE algorithm was used to constrain all covalent bonds involving hydrogen atoms at their equilibrium lengths.

During the FEP simulations, each perturbation converting coniferyl alcohol to either *p*-coumaryl or sinapyl alcohol was divided into 24 windows. For each window, a total of 100 000 MD steps were performed, the first 40 000 being considered equilibration and the remaining 60 000 used for data collection. Probability distribution and free energy convergence plots for few windows are shown in the Supporting Information. FEP simulations were performed for both forward and backward directions. A cumulative total of 4.8 ns of MD was performed for each ligand in water and in the HRPC active site. Lennard-Jones interactions were adjusted linearly over the entire range of λ, the coupling parameter that smoothly connects the initial (λ = 0) and final state (λ = 1) of the perturbed system, i.e., the monolignol. Electrostatic interactions were decoupled for disappearing atoms at λ = 0.5. A soft-core potential was introduced near the λ ends to avoid singularities in the potential. FEP calculations were analyzed using the VMD plugin,[35] and binding free energy differences and statistical errors were calculated using the Bennett acceptance ratio method.[36]

The thermodynamic cycle shown in Scheme 1 was used to calculate the relative binding affinities of the monolignols. $\Delta G_{bind,CA}$ and $\Delta G_{bind,lig}$ represent the binding free energies of coniferyl and the other two ligands (*p*-coumaryl and sinapyl) to the HRPC active site, respectively. ΔG^P and ΔG^W represent the changes in free energy due to transformation of coniferyl alcohol into *p*-coumaryl or sinapyl alcohol inside the active site of enzyme and in water, respectively. The relative binding of

DOI: 10.1021/acs.jpcb.6b00789
J. Phys. Chem. B 2016, 120, 7635−7640

Scheme 1. Thermodynamic Cycle Used To Compute the Relative Binding Affinity of Monolignols to Horseradish Peroxidase[a]

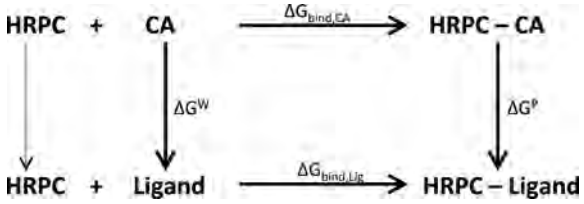

[a]"Ligand" here can be either *p*-coumaryl or sinapyl alcohol.

monolignols was calculated here using ΔG^{P} and ΔG^{W} as $\Delta\Delta G_{bind} = \Delta G_{bind,CA} - \Delta G_{bind,lig} = \Delta G^{P} - \Delta G^{W}$.

To calculate ΔG^{W}, a monolignol with hybrid topology was embedded in a water box of dimensions 30 × 30 × 30 Å^3. The same procedure as in the protein environment was used for the monolignol to calculate the free energy change during transformation of coniferyl to *p*-coumaryl or sinapyl alcohol in aqueous solution.

Docking Calculations. All docking calculations were performed using the Autodock4.2 software.[37] For docking, the apo crystal structure of horseradish peroxidase was used (PDB access code 1ATJ), which does not have any ligand bound to the active site. The *p*-coumaryl, coniferyl, and sinapyl ligands were flexible while the protein was kept rigid during docking simulations. HRPC does not undergo any major structure conformational changes upon ligand binding,[38] and therefore rigid receptor docking should not pose any major problem in evaluating docking results. The CA-RMSD between the apo structure of HRPC and the bound structure (6ATJ.pdb) is 0.27 Å, and there is no major side-chain reorientation of residues lining the active site (Figure SI4).

AutoDockTools1.5.6[37] was used to set the rotatable bonds and add polar hydrogens. Docking was performed using a grid map of 126 in each dimension with 0.375 Å grid spacing. First, for each of the three alcohols, docking calculations were performed with and without the crystal water molecule (W1) in the active site, with a population size of 100; i.e., 100 separate docking calculations were performed for each monolignol using the same apo HRPC structure. Similar results were obtained in both cases in terms of the number of times a monolignol binds in a pose similar to pose C for the three alcohols. Additional docking was performed, with a population size of 1000, for each of the alcohols with either one (W1) or two (W1 and W2) water molecules in the active site. The number of energy evaluations used for each docking calculation was 25 000 000. Clustering analysis was performed using an RMSD tolerance of 2 Å.

π-Stacking Interactions. To analyze the interactions that stabilize binding to the enzyme, only snapshots with the pose C like orientation of the monolignols were considered. Hence, we used the snapshots from the first (for coniferyl) or the last (for *p*-coumaryl or sinapyl) window of the FEP simulations (each 100 ps long; 200 snapshots) to evaluate the monolignol interactions in their binding pose. Two types of interactions were found between the monolignol aromatic ring and the close-by aromatic residues: off-centered parallel displaced stacking and T-shaped.[39] The centroid-centroid distance, R_{cent}, the center-normal angle, θ, and the normal−normal angle, γ, between the aromatic rings[39] were calculated using in-house tcl scripts. Hydrogen bond occupancies between monolignols and water molecules were calculated using a distance cutoff of 3.5 Å and angle cutoff of 30°.

RESULTS

Docking. Blind docking calculations were performed using an apo HRPC structure (1ATJ.pdb) in the resting state to investigate how the three monolignols might bind to the active site of HRPC. Three sets of docking calculations were performed; without and with one (W1) and two (W1 and W2) crystal waters (important for oxidation) in the active site. Docking calculations without water and with W1 produced complexes with monolignol orientations similar to that adopted by the ferulic acid in the crystal structure. However, the presence of two water molecules in the active site negatively affects the binding of the three monolignols, yielding none of the three binding poses seen experimentally. Details of the docking calculations are given in the Supporting Information (Figures SI5 and SI6, Table SI2).

Docking without Crystal Waters. In 70−80% of the docked conformations, the three monolignols bind to the active site in three different orientations, similar to those observed in the crystallographic analysis of ferulic acid bound to HRPC. In the absence of active site waters, we found that in the lowest energy docked complexes the phenolic oxygen in all three monolignols interacts directly with His42 NE2. In contrast, in the case of ferulic acid bound to HRPC (6ATJ), the phenolic oxygen interacts with His42 NE2 via W2 in a pose that primes the substrate for oxidation (pose C).

Docking with Crystal Water W1 in the Active Site near Heme Fe. W1 is present in close proximity to the Fe of the heme porphyrin ring. The lowest binding energy pose for coniferyl has its methoxy group flipped away from Phe179, i.e., opposite to what is seen in the crystal structure for ferulic acid, while for *p*-coumaryl and sinapyl alcohols the phenolic oxygen interacts with His42 as in the case of docking without crystal waters. This means the crystal water W1 does not obstruct the monolignol binding to the peroxidase active site. The pose of the docked monolignols with the phenolic oxygen inside the active site is shown in Figure SI7.

Docking with Two Crystal Waters in the Active Site. Docking of monolignols to HRPC with two waters (W1 and W2) in the active site produced no binding poses resembling any of the three poses observed for ferulic acid. This is because the second crystal water (W2) in the apo structure is located exactly at where the monolignol would bind. We therefore moved this crystal water to its position in the crystal structure of HRPC bound to ferulic acid, thus, in principle, allowing the monolignols to bind and make interactions with active site residues. The water molecules were kept rigid during docking. However, still no binding poses similar to ferulic acid were obtained for any of the monolignols. This is not surprising since it is known to be challenging to include waters in docking calculations, which may enhance or deteriorate the docking results.[40,41]

Overall, in the docking results the following was found: that (1) *p*-coumaryl alcohol binds most frequently to the active site and (2) coniferyl alcohol has the least favorable binding energy. We now further quantify the binding affinity of the three monolignols to the active site of HRPC using more rigorous free energy calculations.

MD-FEP. Free energy perturbation (FEP) calculations were performed in an effort to quantify the relative binding affinities of *p*-coumaryl, coniferyl, and sinapyl alcohols to the active site

DOI: 10.1021/acs.jpcb.6b00789
J. Phys. Chem. B 2016, 120, 7635−7640

of horseradish peroxidase. *p*-Coumaryl alcohol was found to bind most strongly, by −1.3 ± 0.1 kcal/mol compared to coniferyl alcohol, followed by sinapyl alcohol, whose binding free energy was −0.4 ± 0.1 kcal/mol lower than for coniferyl alcohol (Table 1). The trend is consistent with the docking predictions.

Table 1. Binding Affinity of *p*-Coumaryl and Sinapyl Alcohols to HRPC Relative to Coniferyl Alcohol As Calculated from Free Energy Perturbation Calculations

ligand	relative binding affinity (kcal/mol)
coniferyl alcohol	0
p-coumaryl alcohol	−1.3 ± 0.1
sinapyl alcohol	−0.4 ± 0.1

In order to rationalize the relative binding affinities calculated above, we investigated the molecular interactions of the three monolignols with the surrounding protein residues in the active site. We examined two types of interaction that can stabilize monolignol binding: (i) Stacking interactions between the phenyl ring of the monolignols and the three aromatic phenylalanine residues (Phe68, Phe142, and Phe179) that guard the entrance to the active site, especially Phe68 and Phe179 that are more proximal to the substrate. Phe142 is not listed in the table as it is further from monolignols than the cutoff distance of 7 Å used for stacking interaction calculations; (ii) hydrogen bonds between a phenolic group and a water molecule.

As a reference, we also evaluated these two types of interactions (hydrogen bonds and stacking) for ferulic acid bound to HRPC in 6ATJ.pdb. The phenolic −OH group of ferulic acid forms a hydrogen bond with the crystallographic water molecule W2, with an O−O bond distance of 3.18 Å, and W2 also interacts with His42, forming an O−N bond of 3.36 Å in length. The methoxy oxygen on C3 forms a further hydrogen bond, with Arg38 (O−N bond length of 2.89 Å). The methoxy oxygen is considerably less polar than a hydroxyl oxygen and may therefore be expected to form weaker electrostatic interactions with Arg38. For stacking interactions, the calculated centroid−centroid distance, R_{cent}, and the center-normal angle, θ, and the normal−normal angle, γ, between the rings of the ferulic acid and Phe68/Phe179 are shown in Table 2. R_{cent} (8.4/11.1 Å) is much longer than cutoff distance of 7.0 Å. Thus, ferulic acid does not form strong stacking interactions in its bound state.

For coniferyl alcohol, there is hydrogen bond between phenolic −OH and W2 (Figure 2 and Figure SI8). As concerns possible stacking interactions, the average R_{cent} between the coniferyl ring and the Phe68 and Phe179 rings are longer than those in the cases of *p*-coumaryl and sinapyl alcohol (Table 2 and Figure SI9). The average calculated nonbonded interaction between the coniferyl ring and the Phe68 and Phe179 is −4.8 kcal/mol. For sinapyl, the phenolic −OH moves further away from the Heme Fe and W2, interacting with the oxygen atom of Pro139 (Figure 3 and Figure SI8). Stacking interactions may

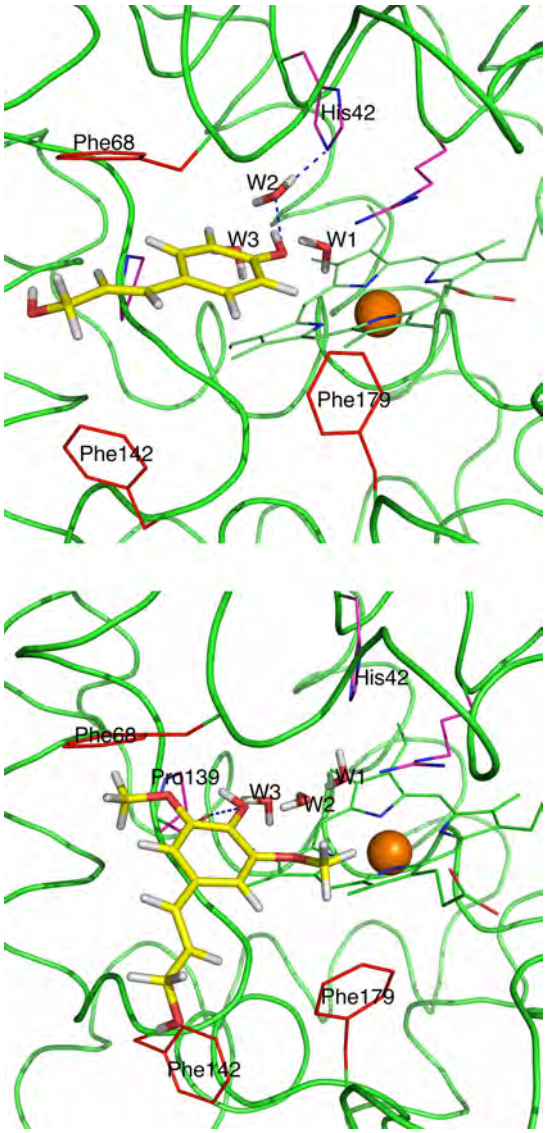

Figure 3. *p*-Coumaryl (upper panel) and sinapyl (lower panel) alcohols bound to the active site of the resting state HRPC enzyme. The blue dashed lines indicate the hydrogen bonds. Protein is in ribbon format. In the case of *p*-coumaryl alcohol, the phenolic −OH (donor) is hydrogen bonded to W2 (acceptor) that further interacts with His42, providing the mechanism for proton transfer during monolignol oxidation. The sinapyl alcohol phenolic −OH group interacts, however, with Pro139.

Table 2. Stacking between the Monolignol and the Nearby Residues Phe68 and Phe179[a]

	Phe68 (parallel-displaced)			Phe179 (T-shaped)		
monolignol	R_{cent} (Å)	θ (deg)	γ (deg)	R_{cent} (Å)	θ (deg)	γ (deg)
ferulic acid	8.41	51	33	11.10	60	76
coniferyl	7.09 ± 0.61	54 ± 6	24 ± 14	6.84 ± 0.48	72 ± 9	79 ± 7
p-coumaryl	6.37 ± 0.50	50 ± 7	27 ± 15	5.94 ± 0.30	75 ± 9	82 ± 5
sinapyl	6.51 ± 0.56	50 ± 7	29 ± 14	6.44 ± 0.37	71 ± 9	77 ± 8

[a]The R_{cent}, θ, and γ are the averages from FEP simulations as described above in the Computational Methods section.

DOI: 10.1021/acs.jpcb.6b00789
J. Phys. Chem. B 2016, 120, 7635−7640

contribute to the binding because the sinapyl ring is mostly outside the active site and closer to the Phe68 ring than that in the case of coniferyl alcohol (Table 2). Correspondingly, the average nonbonded interaction between sinapyl ring and the two aromatic residues is −5.7 kcal/mol.

Three water molecules reside inside the active site when sinapyl is bound compared to two in the case of coniferyl. Also, in sinapyl binding, the more distant Phe142 aromatic ring adopts a different orientation than that in *p*-coumaryl and coniferyl, so as to accommodate the methoxy group at C5 (Figure 3). For *p*-coumaryl both the hydrogen bonding with W2 through the phenolic −OH group and the stacking interaction with Phe68 and Phe179 are present. *p*-Coumaryl also allows three water molecules in the active site, like sinapyl alcohol (Figure 3). The average calculated nonbonded interaction between the *p*-coumaryl ring and the Phe68 and Phe179 rings are −5.07 kcal/mol. Overall, the coniferyl ring has the weakest nonbonded interactions with the guarding Phe residues.

DISCUSSION

In the present FEP simulations and docking calculations the binding affinity is least favorable for coniferyl alcohol. This finding is consistent with weaker interactions between the coniferyl monolignol and the proximal Phe68 and Phe179 residues. As explained in ref 26, the position of the bound monolignols will not change in going from the resting state of HRPC to the active states compounds I and II for the first and the second oxidation during peroxidase-mediated oxidation cycle. W1 in the resting state is replaced by an oxygen atom bound to the Fe forming oxo-iron in compounds I and II, but W2 is still positioned between His42 and Fe. The present binding calculation results, performed in the resting state of enzyme, are thus valid for active states of the peroxidase.

After binding, for efficient oxidation to occur the monolignol needs to be in a pose that facilitates oxidation to occur. Oxidation occurs via a proton-coupled electron transfer mechanism; a water molecule mediates a proton transfer from the phenolic −OH group to His42, and an electron is transferred to the heme Fe or porphyrin ring from the monolignol.[20] Thus, the interactions and distances of the monolignol phenolic oxygen with the water W2 and to heme Fe are essential criteria for productive oxidation.[20] Coniferyl alcohol binds to the active site of HRPC in a pose that fulfils the above criteria (Figure 2 and Figure SI8).

In contrast, the binding poses of *p*-coumaryl and sinapyl alcohols are not optimal. In the case of *p*-coumaryl, although the W2-phenolic −OH hydrogen bond is present, water molecule W3 competes with W2 for hydrogen bonding to the phenolic −OH, thus weakening the important W2-phenolic −OH hydrogen bond. This might negatively affect the proton-transfer step during oxidation.

In the case of sinapyl alcohol, the phenolic −OH group interacts with the Pro139 oxygen (Figure 3). W2 forms a hydrogen bond with phenolic oxygen in which the phenolic oxygen acts as a proton acceptor instead of a proton donor as in the cases of *p*-coumaryl and coniferyl alcohol. Proton transfer from sinapyl thus cannot occur as efficiently as in the cases of coniferyl and *p*-coumaryl.

CONCLUSION

Taken together, our results suggest that the binding affinity of the monolignols decreases in the order of *p*-coumaryl, sinapyl, and coniferyl alcohol. To optimize stacking interactions that stabilize binding, the optimal geometry for oxidation is sacrificed in the cases of *p*-coumaryl and sinapyl alcohols. Our extensive docking and free energy calculations pointed toward the importance of substrate binding pose, which is directly related to the proton transfer step in monolignol oxidation by peroxidase enzyme.

ASSOCIATED CONTENT

Supporting Information

The Supporting Information is available free of charge on the ACS Publications website at DOI: 10.1021/acs.jpcb.6b00789.

Topology and force-field parameters for monolignols and 5-coordinated heme, free energy convergence and detailed docking results, and figures (PDF)

AUTHOR INFORMATION

Corresponding Author

*E-mail Amandeep.k.sangha@vanderbilt.edu; Ph +1 615 936 6594 (A.K.S.).

Present Address

A.K.S.: Chemistry Department, Vanderbilt University, Nashville, TN 37235.

Notes

The authors declare no competing financial interest.

ACKNOWLEDGMENTS

This research was supported by the Bioenergy Science Center, which is a U.S. Department of Energy Bioenergy Research Center supported by the office of Biological and Environmental Research in the Department of Energy Office of Science. This work was conducted using the resources at the National Energy Research Scientific Computing Center (NERSC) under Grants m906 and m1305.

REFERENCES

(1) Freudenberg, K. Biosynthesis and Constitution of Lignin. *Nature* **1959**, *183*, 1152−1155.

(2) Bonawitz, N. D.; Chapple, C. The Genetics of Lignin Biosynthesis: Connecting Genotype to Phenotype. *Annu. Rev. Genet.* **2010**, *44*, 337−363.

(3) Vanholme, R.; Demedts, B.; Morreel, K.; Ralph, J.; Boerjan, W. Lignin Biosynthesis and Structure. *Plant Physiol.* **2010**, *153*, 895−905.

(4) Bonawitz, N. D.; Kim, J. I.; Tobimatsu, Y.; Ciesielski, P. N.; Anderson, N. A.; Ximenes, E.; Maeda, J.; Ralph, J.; Donohoe, B. S.; Ladisch, M.; et al. Disruption of Mediator Rescues the Stunted Growth of a Lignin-Deficient Arabidopsis Mutant. *Nature* **2014**, *509*, 376−380.

(5) Poovaiah, C. R.; Nageswara-Rao, M.; Soneji, J. R.; Baxter, H. L.; Stewart, C. N. Altered Lignin Biosynthesis Using Biotechnology to Improve Lignocellulosic Biofuel Feedstocks. *Plant Biotechnol. J.* **2014**, *12*, 1163−1173.

(6) Fu, C.; Mielenz, J. R.; Xiao, X.; Ge, Y.; Hamilton, C. Y.; Rodriguez, M.; Chen, F.; Foston, M.; Ragauskas, A.; Bouton, J. Genetic Manipulation of Lignin Reduces Recalcitrance and Improves Ethanol Production from Switchgrass. *Proc. Natl. Acad. Sci. U. S. A.* **2011**, *108*, 3803−3808.

(7) Ziebell, A.; Gracom, K.; Katahira, R.; Chen, F.; Pu, Y. Q.; Ragauskas, A.; Dixon, R. A.; Davis, M. Increase in 4-Coumaryl Alcohol Units During Lignification in Alfalfa (Medicago sativa) Alters the

DOI: 10.1021/acs.jpcb.6b00789
J. Phys. Chem. B 2016, 120, 7635−7640

Extractability and Molecular Weight of Lignin. *J. Biol. Chem.* **2010**, *285*, 38961−38968.
(8) Chapple, C.; Ladisch, M.; Meilan, R. Loosening Lignin's Grip on Biofuel Production. *Nat. Biotechnol.* **2007**, *25*, 746−748.
(9) Himmel, M. E.; Ding, S.-Y.; Johnson, D. K.; Adney, W. S.; Nimlos, M. R.; Brady, J. W.; Foust, T. D. Biomass Recalcitrance: Engineering Plants and Enzymes for Biofuels Production. *Science* **2007**, *315*, 804−807.
(10) Tschaplinski, T. J.; Standaert, R. F.; Engle, N. L.; Martin, M. Z.; Sangha, A. K.; Parks, J. M.; Smith, J. C.; Samuel, R.; Pu, Y.; Ragauskas, A. J.; et al. Down-Regulation of the Caffeic Acid O-methyltransferase Gene in Switchgrass Reveals a Novel Monolignol Analog. *Biotechnol. Biofuels* **2012**, *5* (1), 71.
(11) Li, X.; Chapple, C. Understanding Lignification: Challenges Beyond Monolignol Biosynthesis. *Plant Physiol.* **2010**, *154* (2), 449−452.
(12) Hofte, H.; Sibout, R. Plant Cell Biology: The ABC of Monolignol Transport. *Curr. Biol.* **2012**, *22* (13), R533−R535.
(13) Nielsen, K. L.; Indiani, C.; Henriksen, A.; Feis, A.; Becucci, M.; Gajhede, M.; Smulevich, G.; Welinder, K. G. Differential Activity and Structure of Highly Similar Peroxidases. Sepctroscopic, Crystallographic, and Enzymatic Analyses of Lignifying Arabidopsis Thaliana Peroxidase A2 and Horseradish Peroxidase A2. *Biochemistry* **2001**, *40*, 11013−11021.
(14) Kobayashi, T.; Taguchi, H.; Shigematsu, M.; Tanahashi, M. Substitient Effects of 3,5-Disubstituted p-Coumaryl Alcohols on Their Oxidation Using Horseradish Peroxidase-H_2O2 as the Oxidant. *J. Wood Sci.* **2005**, *51*, 607−614.
(15) Sangha, A. K.; Parks, J. M.; Standaert, R. F.; Ziebell, A.; Davis, M.; Smith, J. C. Radical Coupling Reactions in Lignin Synthesis: A Density Functional Theory Study. *J. Phys. Chem. B* **2012**, *116*, 4760−4768.
(16) Fagerstedt, K. V.; Kukkola, E. M.; Koistinen, V. V. T.; Takahashi, J.; Marjamaa, K. Cell Wall Lignin is Polymerized by Class III Secretable Plant Peroxidases in Norway Spruce. *J. Integr. Plant Biol.* **2010**, *52* (2), 186−194.
(17) Brunow, G.; Kilpelainen, I.; Sipila, J.; Syrjanen, K.; Karhunen, P.; Setala, H.; Rummakko, P. Oxidative Coupling of Phenols and The Biosynthesis of Lignin. *ACS Symp. Ser.* **1998**, *697*, 131−147.
(18) Sangha, A. K.; Davison, B. H.; Standaert, R. F.; Davis, M. F.; Smith, J. C.; Parks, J. M. Chemical Factors that Control Lignin Polymerization. *J. Phys. Chem. B* **2014**, *118* (1), 164−170.
(19) Dunford, H. B.; Adeniran, A. J. Hammett Rho Sigma Correlation for Reactions of Horseradish Peroxidase Compound II with Phenols. *Arch. Biochem. Biophys.* **1986**, *251* (2), 536−42.
(20) Derat, E.; Shaik, S. An Efficient Proton-Coupled Electron-Transfer Process During Oxidation of Ferulic Acid by Horseradish Peroxidase: Coming Full Cycle. *J. Am. Chem. Soc.* **2006**, *128*, 13940−13949.
(21) Chipot, C.; Pohorille, A. *Free Energy Calculations. Theory and Applications in Chemistry and Biology*; Springer Verlag: 2007.
(22) Pohorille, A.; Jarzynski, C.; Chipot, C. Good Practices in Free-Energy Calculations. *J. Phys. Chem. B* **2010**, *114* (32), 10235−10253.
(23) Mobley, D. L.; Shirts, M. R. An Introduction to Best Practices in Free Energy Calculations. In *Biomolecular Simulations: Methods and Protocols*; Springer: 2013; Vol. *924*, pp 271−311.
(24) Klimovich, P. V.; Shirts, M. R.; Mobley, D. L. Guidelines for the Analysis of Free Energy Calculations. *J. Comput.-Aided Mol. Des.* **2015**, *29* (5), 397−411.
(25) Henriksen, A.; Smith, A. T.; Gajhede, M. The Structures of the Horseradish Peroxidase C-Ferulic Acid Complex and the Ternary Complex with Cyanide Suggest How Peroxidases Oxidize Small Phenolic Substrates. *J. Biol. Chem.* **1999**, *274* (49), 35005−35011.
(26) Humphrey, W.; Dalke, A.; Schulten, K. VMD: Visual Molecular Dynamics. *J. Mol. Graphics* **1996**, *14* (1), 33−38.
(27) Phillips, J. C.; Braun, R.; Wang, W.; Gumbart, J.; Tajkhorshid, E.; Villa, E.; Chipot, C.; Skeel, R. D.; Kale, L.; Schulten, K. Scalable Molecular Dynamics with NAMD. *J. Comput. Chem.* **2005**, *26* (16), 1781−1802.
(28) MacKerell, A. D.; Bashford, D.; Bellott, M.; Dunbrack, R. L.; Evanseck, J. D.; Field, M. J.; Fischer, S.; Gao, J.; Guo, H.; Ha, S.; et al. All-atom Empirical Potential for Molecular Modeling and Dynamics Studies of Proteins. *J. Phys. Chem. B* **1998**, *102* (18), 3586−3616.
(29) Mackerell, A. D.; Feig, M.; Brooks, C. L. Extending the Treatment of Backbone Energetics in Protein Force Fields: Limitations of Gas-phase Quantum Mechanics in Reproducing Protein Conformational Distributions in Molecular Dynamics Simulations. *J. Comput. Chem.* **2004**, *25* (11), 1400−1415.
(30) Jorgensen, W. L.; Chandrasekhar, J.; Madura, J. D.; Impey, R. W.; Klein, M. L. Comparison of Simple Potential Functions for Simulating Liquid Water. *J. Chem. Phys.* **1983**, *79*, 926.
(31) Petridis, L.; Smith, J. C. A Molecular Mechanics Force Field for Lignin. *J. Comput. Chem.* **2009**, *30* (3), 457−467.
(32) Vanommeslaeghe, K.; Hatcher, E. R.; Acharya, C.; Kundu, S.; Zhong, S.; Shim, J.; Darian, E.; Guvench, O.; Lopes, P.; Vorobyov, I.; et al. CHARMM General Force Field (CGenFF): A Force Field for Drug-Like Molecules Compatible with the CHARMM All-Atom Additive Biological Force Fields. *J. Comput. Chem.* **2010**, *31* (4), 671−690.
(33) Feller, S. E.; Zhang, Y.; Pastor, R. P.; Brooks, B. R. Constant Pressure Molecular Dynamics Simulation: The Langevin Piston Method. *J. Chem. Phys.* **1995**, *103* (11), 4613.
(34) Darden, T.; York, D.; Pedersen, L. Particle Mesh Ewald - an N.Log(N) Method for Ewald Sums in Large Systems. *J. Chem. Phys.* **1993**, *98* (12), 10089−10092.
(35) Liu, P.; Dehez, F.; Cai, W. S.; Chipot, C. A Toolkit for the Analysis of Free-Energy Perturbation Calculations. *J. Chem. Theory Comput.* **2012**, *8* (8), 2606−2616.
(36) Bennett, C. H. Efficient Estimation of Free-Energy Differences from Monte-Carlo Data. *J. Comput. Phys.* **1976**, *22* (2), 245−268.
(37) Morris, G. M.; Huey, R.; Lindstrom, W.; Sanner, M. F.; Belew, R. K.; Goodsell, D. S.; Olson, A. J. AutoDock4 and AutoDockTools4: Automated Docking with Selective Receptor Flexibility. *J. Comput. Chem.* **2009**, *30* (16), 2785−2791.
(38) Laberge, M.; Osvath, S.; Fidy, J. Aromatic Substrate Specificity of Horseradish Peroxidase C Studied by A Combined Fluorescence Line Narrowing/Energy Minimization Approach: The Effect of Localized Side-Chain Reorganization. *Biochemistry* **2001**, *40* (31), 9226−37.
(39) McGaughey, G. B.; Gagne, M.; Rappe, A. K. Pi-Stacking Interactions - Alive and Well in Proteins. *J. Biol. Chem.* **1998**, *273* (25), 15458−15463.
(40) Kumar, A.; Zhang, K. Y. J. Investigation on the Effect of Key Water Molecules on Docking Performance in CSARdock Exercise. *J. Chem. Inf. Model.* **2013**, *53* (8), 1880−1892.
(41) Lemmon, G.; Meiler, J. Towards Ligand Docking Including Explicit Interface Water Molecules. *PLoS One* **2013**, *8* (6), e67536.

DOI: 10.1021/acs.jpcb.6b00789
J. Phys. Chem. B 2016, 120, 7635−7640